

Simulation of nitrogen emissions in a low swirl burner

J. B. Bell, M. S. Day, X. Gao, M. J. Lijewski

Center for Computational Science and Engineering
Lawrence Berkeley National Laboratory

Abstract. We present simulations of a laboratory-scale low swirl burner fueled with hydrogen at atmospheric pressure. The study uses detailed chemistry and transport including a sub-mechanism for computing nitrogen emissions. The simulation shows how the cellular burning structures characteristic of lean premixed hydrogen combustion lead to enhancements in the NO_x emissions from these flames. Analysis of the simulation data illustrates the chemical pathways that lead to nitrogen emissions and how they are enhanced within local regions of intense burning.

1. Introduction

Combustion devices based on lean premixed flames generate substantially lower NO_x emissions than equivalent nonpremixed or stoichiometric premixed systems [3]. For lean premixed systems, the reduction in NO_x emissions is believed to be a direct consequence of the lower post-flame gas temperatures. Recent laboratory experiments have shown that ultra-lean hydrocarbon flames (with fuel concentrations well below lean blow-off limits) can in fact be stabilized in a turbulent burner if the fuel mixture is enriched with H₂ [8]. Hydrogen addition enhances the effective flame speed and auto-ignition processes of the mixture [7], both of which lead to an increased resistance to strain-induced extinction. However, NO_x emissions do not decrease uniformly with increasing hydrogen enrichment relative to the hydrocarbon fuel. In a recent experimental study [2], pure H₂-air flames at 8 atmospheres exhibited a pronounced “floor” at 1 ppm NO in the exhaust stream, below which further reduction in the adiabatic post-flame gas temperature had no effect on the measured emissions. Moreover, this “floor” was a factor of two or three higher than values produced in the same burner using ultra-lean hydrocarbon mixtures (seeded with hydrogen) that had comparable post-flame gas temperatures.

Here, we simulate a laboratory scale model of a low swirl burner fueled by hydrogen at an equivalence ratio of $\phi = 0.37$ at atmospheric pressure with nitrogen emissions chemistry. Our goal is to identify the underlying mechanism that controls the formation of nitrogen emissions in this type of flame. To accurately capture the emissions formation and dynamics, simulations are performed with a detailed kinetics model for hydrogen chemistry including the relevant nitrogen chemistry and detailed transport. The simulations fully resolve the turbulent flow and internal flame structure so that no model for turbulence/chemistry is required.

2. Numerical Methodology

The simulations presented here are based on a low Mach number formulation [13,9] of the reacting Navier-Stokes equations. The methodology treats the fluid as a mixture of perfect gases ignoring Soret, Dufour and radiative transport processes. We use a mixture-averaged model for differential species diffusion, which is critical for capturing the thermodiffusive behavior of lean hydrogen flames

(see [6] for a complete discussion of this approximation). A detailed chemical description containing 15 species and 58 reversible Arrhenius reactions is used to describe premixed hydrogen-air combustion and subsequent NO_x formation. This mechanism was derived by rate-of-production and sensitivity analyses from a full reaction mechanism [10,11] to obtain the minimum reaction set that describes NO formation in H_2 oxidation at lean conditions. It includes NO formation routes through NNH and N_2O , as well as the thermal mechanism. The reactions involving nitrogen emission are presented in Table 1. Additional detail along with two dimensional studies of NO_x emissions in H_2 flames at various equivalence ratios are presented in [1].

Table 1. Thermal and $\text{NNH}/\text{N}_2\text{O}$ formation routes for NO . For each reaction, i , the forward progress rate $k_i = A_i T^{n_i} \exp(-E_i/RT)$ (moles/cm³ · s), where A_i , n_i , E_i , (cal/g · K) are given below.

No.	Reaction	A	n	E	No.	Reaction	A	n	E
30	$\text{NO} + \text{O} (+\text{M}) \rightleftharpoons \text{NO}_2 (+\text{M})$	1.3E15	-0.75	0	45	$\text{NH} + \text{NO} \rightleftharpoons \text{N}_2\text{O} + \text{H}$	-2.2E13	-0.23	0
31	$\text{NO} + \text{HO}_2 \rightleftharpoons \text{NO}_2 + \text{OH}$	2.1E12	0.00	-497	46	$\text{NH} + \text{NO} \rightleftharpoons \text{N}_2 + \text{OH}$	2.2E13	-0.23	0
32	$\text{NO}_2 + \text{H} \rightleftharpoons \text{NO} + \text{OH}$	1.3E14	0.00	362	47	$\text{NH} + \text{NO}_2 \rightleftharpoons \text{N}_2\text{O} + \text{OH}$	1.0E13	0.00	0
33	$\text{NO}_2 + \text{O} \rightleftharpoons \text{NO} + \text{O}_2$	1.1E14	-0.52	0	48	$\text{N} + \text{OH} \rightleftharpoons \text{NO} + \text{H}$	3.8E13	0.00	0
34	$2 \text{NO}_2 \rightleftharpoons 2 \text{NO} + \text{O}_2$	4.5E12	0.00	27599	49	$\text{N} + \text{O}_2 \rightleftharpoons \text{NO} + \text{O}$	6.4E09	1.00	6280
35	$\text{N}_2\text{O} (+\text{M}) \rightleftharpoons \text{N}_2 + \text{O} (+\text{M})$	1.3E12	0.00	62570	50	$\text{N} + \text{NO} \rightleftharpoons \text{N}_2 + \text{O}$	2.1E13	0.00	0
36	$\text{N}_2\text{O} + \text{H} \rightleftharpoons \text{N}_2 + \text{OH}$	3.3E10	0.00	4729	51	$\text{NNH} \rightleftharpoons \text{N}_2 + \text{H}$	6.5E07	0.00	0
37	$\text{N}_2\text{O} + \text{H} \rightleftharpoons \text{N}_2 + \text{OH}$	4.4E14	0.00	19254	52	$\text{NNH} + \text{H} \rightleftharpoons \text{N}_2 + \text{H}_2$	1.0E14	0.00	0
38	$\text{N}_2\text{O} + \text{O} \rightleftharpoons \text{NO} + \text{NO}$	9.2E13	0.00	27679	53	$\text{NNH} + \text{O} \rightleftharpoons \text{N}_2\text{O} + \text{H}$	1.0E14	0.00	0
39	$\text{N}_2\text{O} + \text{O} \rightleftharpoons \text{N}_2 + \text{O}_2$	3.7E12	0.00	15936	54	$\text{NNH} + \text{O} \rightleftharpoons \text{N}_2 + \text{OH}$	8.0E13	0.00	0
40	$\text{NH} + \text{H} \rightleftharpoons \text{N} + \text{H}_2$	3.0E13	0.00	0	55	$\text{NNH} + \text{O} \rightleftharpoons \text{NH} + \text{NO}$	5.0E13	0.00	0
41	$\text{NH} + \text{O} \rightleftharpoons \text{NO} + \text{H}$	9.2E13	0.00	0	56	$\text{NNH} + \text{OH} \rightleftharpoons \text{N}_2 + \text{H}_2\text{O}$	5.0E13	0.00	0
42	$\text{NH} + \text{OH} \rightleftharpoons \text{N} + \text{H}_2\text{O}$	5.0E11	0.50	2000	57	$\text{NNH} + \text{O}_2 \rightleftharpoons \text{N}_2 + \text{HO}_2$	2.0E14	0.00	0
43	$\text{NH} + \text{O}_2 \rightleftharpoons \text{NO} + \text{OH}$	1.3E06	1.50	100	58	$\text{NNH} + \text{O}_2 \rightleftharpoons \text{N}_2 + \text{H} + \text{O}_2$	5.0E13	0.00	0
44	$\text{NH} + \text{NO} \rightleftharpoons \text{N}_2\text{O} + \text{H}$	2.9E14	-0.40	0					

The numerical methodology uses a finite-volume numerical discretization [4] that combines a symmetric operator-split treatment of chemistry and transport with a density-weighted approximate projection method to impose the low Mach number constraint. The integration proceeds on the time scale of the advective transport; faster diffusion and chemistry processes are treated implicitly in time. The integration scheme is embedded in an adaptive mesh refinement algorithm based on a hierarchical system of rectangular grid patches. The complete integration algorithm is second-order accurate in space and time, and discretely conserves species mass and enthalpy. The methodology is implemented in parallel using a hybrid programming model. Patches of data are distributed over nodes using a coarse-grained load distribution strategy based on MPI. Within nodes, fine-grained parallelization within patches is implemented using a thread-based approach using OpenMP. The hybrid implementation scales well to 50K processors.

The configuration uses a 2.5 cm radius nozzle with mean flow specified from experimental measurements provided by Petersson et al. [12] for a case with mean flow of 6 m/s, scaled uniformly by 250% to approximate profiles at a higher fueling rate of 15 m/s. Turbulent fluctuations matched to experimentally measured turbulent intensities and integral length scales are added to the mean flow. Outside the nozzle, a 35 cm/s upward coflow of air at 300K is imposed.

The simulation domain measures 25 cm × 250 cm × 25 cm and is discretized using a base mesh of 256³. Three levels of grid refinement, each by a factor of 2, dynamically track regions of high vorticity (turbulence) and reactivity (combustion/flame), and the resulting effective resolution is 2048³. Note that this configuration, and the simulation parameters, are identical to the high-turbulence lean hydrogen case discussed in [5], except for the inclusion of detailed emission chemistry. In that work, we demonstrated that this level of resolution is adequate to capture the detailed structure of the flame including the peak fuel consumption, the thermal field and major species.

3. Simulations Result and Analysis

The inclusion of emissions chemistry does not change the basic flame structure, which is described in [5]. The overall flame shape and structure of the NO profile are shown in Figure 1. Here, we focus on the details of the nitrogen chemistry in the core of the flame above the nozzle, specifically for $r < 2.5$ cm. For this analysis, we construct a local coordinate system around the flame using T as a progress variable. We identify the flame surface with the $T = 1144$ isotherm and extend the coordinate system on either side by following integral curves of ∇T . We then construct a triangularization of the original surface. For each triangle, we extend off the surface to form tubes with triangular cross-section which we will refer to as “flamelets.” We then sample T , fuel consumption and reaction rates associated with the nitrogen chemistry over each flamelet, which are then sorted and binned according to the peak fuel consumption rate, and conditionally averaged in temperature space.

Figure 2(a) shows the distribution of burning strength bins where they intersect the $T = 1144$ K isotherm. For several representative bins, Figures 2(b–d) show conditional mean NO production rates with temperature for the dominant contributors using the numbering in Table 1. The conditional mean total NO production rate (shown as the solid black line in the Figure 2) consists primarily of contributions from the “thermal” ($\omega_{\text{NO-therm}}$, dotted black line) and NNH ($\omega_{\text{NO-NNH}}$, dashed black line) routes. The thermal route consists of three reactions that create NO from O_2 , N_2 , and the N radical; these are typically associated with high temperature ($T \gtrsim 1700$). The NNH route is initiated when N_2 combines with H to form NNH. NNH then reacts to produce either N_2O or the pair, NO and NH. Of the N_2O created, approximately 90% is converted back to N_2 , and the remainder reacts to NO. The NH reacts to N, and then proceeds to NO through the thermal route. Even though most of the nitrogen passing through the NNH route is recycled back to N_2 , the fraction that reacts to NO still accounts the bulk of the NO production. It is interesting that both the NNH and thermal rates become significant when $T \gtrsim 1300$; the adiabatic flame temperature for this fuel mixture is 1360 K, and peak temperatures are observed in excess of 1740 K across all flamelet groups. Similar increases in NO production by the NNH and thermal routes were observed in methane-air mixtures seeded with H_2 [7].

Figure 2 suggests that although the strongest burning regions produce NO at a rate that is as high as 20 times that of the weakly burning regions at comparable temperatures, most of the flame is actually burning at relatively weak rates. Figure 3(a) shows integrated NO production as a function of T , showing that the majority of NO is generated near 1500 K. Also, we see that $\approx 80\%$ of the NO is created through the NNH route, while $\approx 20\%$ is generated via the thermal route. Figure 3(b) shows a quantitative reaction path diagram, where the thickness of the graph edges is scaled to the transfer rate of nitrogen atoms between species pairs. The data is integrated over the flame region where $r < 2.5$ cm, and over the entire temperature range. Contributions to each edge are collected into 3 burning groups (see caption), and represented as percentages of total NO production. The $\text{N}_2 \rightarrow \text{N}_2\text{O}$ path shows a negative contribution for the weak flames, indicating that the path actually reverses. In spite of the extremely large NO production rates in the hotspot regions, the weakly burning parts of the flame account for over half of the total NO production.

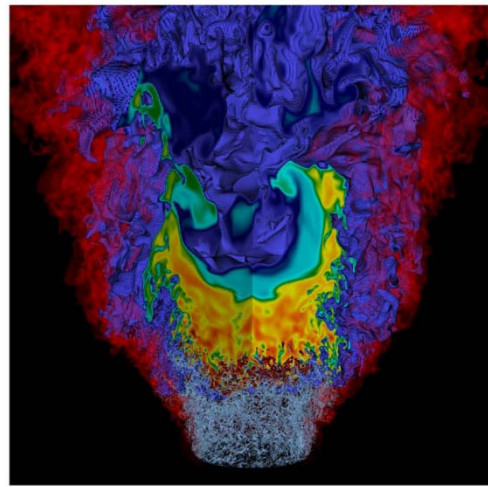


Figure 1. Cutaway of flame snapshot. Isovolume (enclosed in blue, colored on exposed surfaces) of NO concentration, fuel boundary is semi-opaque red surface, and grey represents vertical structures at shear layer of turbulent swirling flow.

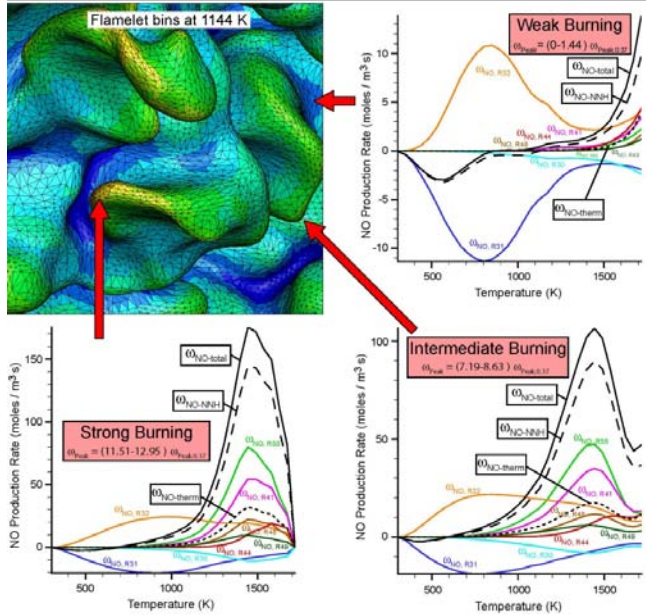


Figure 2. Emission chemistry in a turbulent lean hydrogen-air low-swirl flame. The flame surface is divided into local flamelets, and binned by peak burning rate. (a) $T = 1144\text{K}$, colored where it intersects the flamelets by corresponding bin number (blue = 1, red = 10). (b–d) Conditional mean rates for the dominant reactions producing NO, along with the total NO production (black curve). Dotted black curves represent the total contribution due to the “thermal” sub-mechanism; dashed curves indicate the total due to the NNH sub-mechanism.

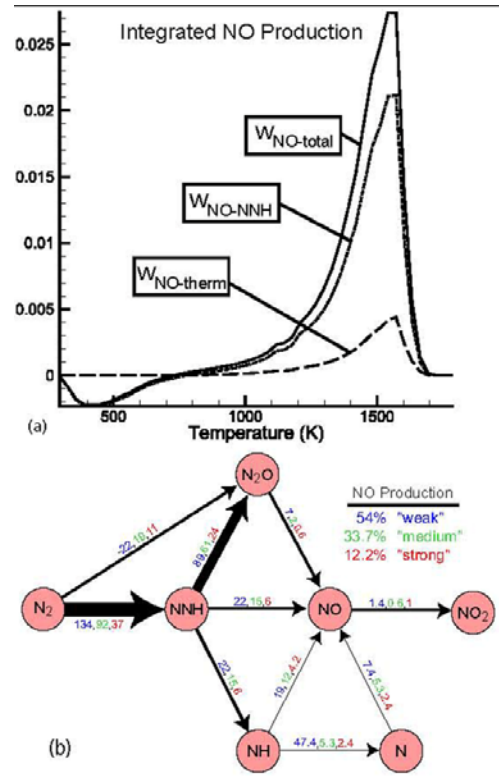


Figure 3. (a) Distribution of integrated emissions production and (b) Path diagram quantifying the integrated transfer rate of N atoms between species, normalized by the total rate of N atoms into NO. Each path indicates the contribution (in percent of NO production rate) from the weak ($\omega_{\text{Peak}} = 0 - 4\omega_{\text{Peak},0.37}$, blue), intermediate ($\omega_{\text{Peak}} = 4 - 9\omega_{\text{Peak},0.37}$, green) and strong ($\omega_{\text{Peak}} = 9 - 13\omega_{\text{Peak},0.37}$, red) flames, where $\omega_{\text{Peak},0.37}$ is the peak consumption rate of the flat flame at $\phi = 0.37$.

The premixed hydrogen flame simulated here shows the cellular structure characteristic of thermodynamically unstable flames. These cellular structures lead to significant enhancement in the local burning and, not surprisingly, increases in the level of nitrogen emissions. Local flamelet analysis confirms this behavior and that the dominant pathway is through NNH. Similar results were shown in [1]; however, the more intense turbulence here leads to increased emissions.

Future work will examine the emissions chemistry in greater detail including NO_2 formation and emissions characteristics in the shear-layer region of the nozzle flow. Finally, we will look at the effects of elevated pressure and a range of equivalence ratios in order to confirm that the processes we have identified are applicable to the experimental data showing the NO_x floor.

References

- [1] J. B. Bell, M. S. Day, X. Gao, and P. Glarborg. Numerical simulation of nitrogen oxide formation in lean premixed turbulent $H_2/O_2/N_2$ flames. *Proc. Combust. Inst.*, 33:to appear, 2010.
- [2] R. K. Cheng, D. Littlejohn, P. A. Strakey, and T. Sidwell. Laboratory investigation of a low-swirl injector with H_2 and CH_4 at gas turbine conditions. *Proc. Combust. Inst.*, 32:3001–3009, 2009.
- [3] S. M. Correa. A review of NO_x formation under gas-turbine combustion conditions. *Combust. Sci. Technol.*, 87:329–362, 1992.
- [4] M. S. Day and J. B. Bell. Numerical simulation of laminar reacting flows with complex chemistry. *Combust. Theory Modelling*, 4:535–556, 2000.
- [5] M. S. Day, J. B. Bell, R. K. Cheng, S. Tachibana, V. E. Beckner, and M. J. Lijewski. *Cellular burning in lean premixed turbulent hydrogen-air flames: coupling experimental and computational analysis at the laboratory scale, volume 180 of Journal of Physics Conference Series: SciDAC 2009* (W. Tang, Ed.). Institute of Physics Publishing, San Diego, CA, 2009.
- [6] A. Ern and V. Giovangigli. *Multicomponent Transport Algorithms, volume m24 of Lecture Notes in Physics*. Springer-Verlag, Berlin, 1994.
- [7] E. R. Hawkes and J. H. Chen. Direct numerical simulation of hydrogen-enriched lean premixed methane-air flames. *Combust. Flame*, 138:242–258, 2004.
- [8] D. Littlejohn and R. K. Cheng. Fuel effects on a low-swirl injector for lean premixed gas turbines. *Proc. Combust. Inst.*, 31:3155–3162, 2007.
- [9] A. Majda and J. A. Sethian. The derivation and numerical solution of the equations for zero Mach number combustion. *Combust. Sci. Technol.*, 42:185–205, 1985.
- [10] T. Mendiara and P. Glarborg. Ammonia chemistry in oxy-fuel combustion of methane. *Combust. Flame*, 156:1937–1949, 2009.
- [11] T. Mendiara and P. Glarborg. Reburn chemistry in oxy-fuel combustion of methane. *Energ. Fuels*, 23:3565–3572, 2009.
- [12] P. Petersson, J. Olofsson, C. Brackman, H. Seyfried, J. Zetterberg, M. Richter, M. Alden, M. Linne, R. Cheng, A. Nauert, D. Geyer, and A. Dreizler. Simultaneous PIV/OH PLIF, Rayleigh thermometry/OH PLIF and stereo PIV measurements in a low-swirl flame. *Appl. Opt.*, 46:3928–3936, 2007.
- [13] R. G. Rehm and H. R. Baum. The equations of motion for thermally driven buoyant flows. *N. B. S. J. Res.*, 83:297–308, 1978.